



UNIVERSIDADE ESTADUAL DE CAMPINAS
SISTEMA DE BIBLIOTECAS DA UNICAMP
REPOSITÓRIO DA PRODUÇÃO CIENTÍFICA E INTELLECTUAL DA UNICAMP

Versão do arquivo anexado / Version of attached file:

Versão do Editor / Published Version

Mais informações no site da editora / Further information on publisher's website:

<https://www.sciencedirect.com/science/article/pii/S0261306914005299>

DOI: 10.1016/j.matdes.2014.07.002

Direitos autorais / Publisher's copyright statement:

©2014 by Elsevier. All rights reserved.

DIRETORIA DE TRATAMENTO DA INFORMAÇÃO

Cidade Universitária Zeferino Vaz Barão Geraldo

CEP 13083-970 – Campinas SP

Fone: (19) 3521-6493

<http://www.repositorio.unicamp.br>



Interconnection of thermal parameters, microstructure, macrosegregation and microhardness of unidirectionally solidified Zn-rich Zn–Ag peritectic alloys



Marcelino Dias^a, Crystopher Brito^a, Felipe Bertelli^a, Otávio L. Rocha^b, Amauri Garcia^{a,*}

^a Department of Manufacturing and Materials Engineering, University of Campinas, UNICAMP, 13083-970 Campinas, SP, Brazil

^b Federal Institute of Education, Science and Technology of Pará, IFPA, Almirante Barroso Avenue 1155, 66093-020 Belém, PA, Brazil

ARTICLE INFO

Article history:

Received 17 May 2014

Accepted 2 July 2014

Available online 14 July 2014

Keywords:

Solidification

Microstructure

Peritectic Zn–Ag alloys

Macrosegregation

Microhardness

ABSTRACT

In this work, the microstructural evolution of Zn–3.2 wt%Ag (hypoperitectic) and Zn–8 wt%Ag (hyperperitectic) alloys during transient unidirectional solidification is investigated. The experimental results include solidification thermal parameters such as the growth rate (V_L), thermal gradient (G_L) and tip cooling rate (\dot{T}), which are related to the microstructural interphase spacing (λ) by proposed experimental growth laws. It is shown that, the classical lamellar eutectic growth law $\lambda^2 V = \text{constant}$, applies to the growth of the peritectic Zn–Ag alloys examined, despite the different values of the constant associated with each alloy composition. In contrast, it is shown that identical functions of the form $\lambda = \text{constant} (G_L)^{-1/4} (V_L)^{-1/8}$, and $\lambda = \text{constant} (\dot{T}^{-1/3})$ can be applied to both alloys examined. Positive solute macrosegregation was observed in regions close to the bottom of the castings. The dependence of microhardness (HV) on the length scale of the microstructures (including that of a single phase Zn 0.8 wt%Ag alloy: λ_c – cellular spacing) is examined. An experimental Hall–Petch type power law is proposed relating the resulting microhardness to λ_c for the single phase alloy, and despite the segregation profiles and the alloying differences of the hypoperitectic and hyperperitectic alloys, the average microhardnesses of these alloys is shown to be essentially constant and similar along the castings lengths.

© 2014 Elsevier Ltd. All rights reserved.

1. Introduction

Peritectic and eutectic reactions can be found in metallic, organic and inorganic materials. The peritectic invariant transformation occurs on cooling of a liquid phase (L) with a primary solid phase (α) to form a second solid phase (β) below the peritectic temperature. A competitive growth occurs with the dissolution of the primary phase, to permit the second phase to freeze out from the liquid, i.e. the peritectic reaction will occur where these three phases are in contact (an equilibrium situation that is generally not observed in practice). In another growth mechanism, called the peritectic transformation, once the α phase is enveloped by β , additional transformation is controlled by diffusion through the β phase [1–3]. However, a variety of microstructures can be obtained from during solidification of peritectic alloys under non-equilibrium conditions, which depend mainly on the thermal parameters during solidification (thermal gradient, G_L , growth rate, V_L , and cooling rate, \dot{T}) and the nucleation conditions. Possible microstructures include: cellular

[4], bands [5,6], lamellar [7], eutectic type structures [8], and dendritic structures [9].

Zinc-based alloys are used in the manufacture of a number of components of the electrical/electronics industry, e.g. connectors, mobile-phone antennae, transformer cores, heat sinks, shutter mechanisms in cameras, applications requiring electromagnetic shielding, etc. [10]. Despite the importance of Zn-based alloys, studies focusing on correlations between solidification thermal parameters, microstructures of peritectic Zn–Cu and Zn–Ag alloys, and application properties are sparse. Ma et al. [11,12], carried out studies on steady-state growth of Zn-rich Zn–Cu alloys for a range of compositions between 1.53 and 7.37 wt%Cu. They reported the occurrence of two-phase regular and plate-like cellular microstructures in a range of compositions near the peritectic point. Brito et al. [4,13], carried out transient solidification experiments on Zn–1.0 wt%Cu (single-phase) and Zn–2.2 wt%Cu (hypoperitectic) alloys, in which experimental growth laws relating the length scale of the cellular microstructure to solidification thermal parameters are proposed [4] and microstructural features and macrosegregation are related to the alloys microhardnesses [13]. The electrochemical corrosion behavior of a peritectic Zn–Cu alloys as a

* Corresponding author. Tel.: +55 19 3521 3320; fax: +55 19 3289 3722.

E-mail address: amaurig@fem.unicamp.br (A. Garcia).

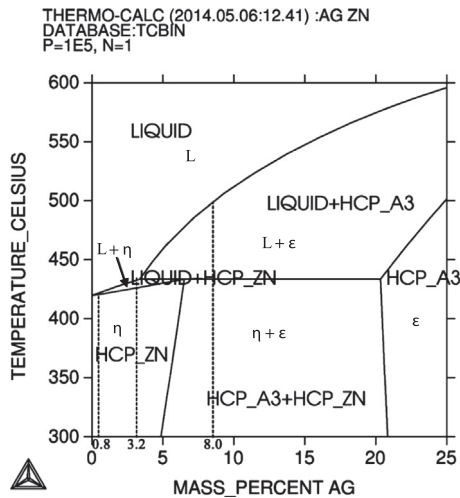


Fig. 1. Partial Zn–Ag phase diagram: the dotted lines indicate the alloys examined in the present study.

function of both solute macrosegregation and the size of cellular spacings has been examined in a recent study by Osório et al. [14].

Concerning Zn–Ag alloys, the first study on solidification of peritectic alloys was conducted by Uhlmann and Chadwick [15]. They investigated Zn-rich Zn–Ag peritectic alloys and pointed out that the characteristic microstructure was formed by dendrites of a primary phase embedded in a matrix of peritectic phase. Xu et al. [16,17] carried out rapid solidification experiments to investigate the microstructural pattern of Zn-rich Zn–Ag peritectic alloys containing up to 9.0 at.%Ag. These authors, for comparison, have also performed steady-state Bridgman growth on the same alloys. They reported that instead of a typical microstructure formed by dendrites of the primary phase surrounded by the peritectic phase, a two-phase plate like microstructure, with or without dendrites of the primary phase, was observed for growth rates higher than a critical value. In a recent study on transient solidification of a single-phase Zn–0.8 wt%Ag alloy, the resulting microstructure was reported to be formed by regular cells, however, for cooling rates higher than 10 °C/s a plate-like cellular morphology was observed [18]. An experimental growth law relating the cell spacing with the cooling rate has been proposed, which was shown to be able to represent both the steady-state and transient growth regimes of single-phase Zn–Ag alloys.

Despite the aforementioned studies on microstructural selection in peritectic Zn-based alloys solidification, the effects of transient heat flow conditions on the microstructural length scales of

these alloys remain less well explored, especially studies encompassing the effects of macrosegregation and of the resulting microstructural pattern on mechanical and chemical properties. Most of the experimental studies existing in the literature on peritectic alloys, have been carried out under steady-state solidification, where both thermal gradient and growth rate can be independently controlled and kept constant in time. However, studies on directional solidification of peritectic alloys under transient heat flow conditions, in which both the thermal gradient and growth rate vary freely in time and are interdependent, are scarce. The main purpose of the present work is to analyze the effects of the cooling rate and macrosegregation during transient solidification on the microstructural evolution of peritectic Zn–Ag alloys. It is also aimed to relate the resulting microstructural length scale and local composition to the corresponding microhardness, including for a single-phase Zn–Ag alloy for comparative purposes.

2. Experimental procedure

Transient unidirectional solidification (DS) experiments were carried out with Zn-rich Zn–Ag alloys, containing 0.8 wt%Ag (single-phase), 3.2 wt%Ag (hypoperitectic) and 8 wt%Ag (hyperperitectic), as indicated in the phase diagram of Fig. 1, in order to permit transient solidification thermal parameters to be correlated with microstructural features. To promote directional growth under a wide range of cooling rates, the experiments were conducted in an experimental setup consisting of a water-cooled mold with heat being extracted from the bottom, promoting vertical upward directional solidification, as detailed in previous articles [19,20]. The stainless steel mold had an internal diameter of 50 mm, height of 110 mm and wall thickness of 3 mm. The bottom part of the mold was closed with a thin (3 mm thick) carbon steel sheet, which physically separates the metal from the cooling water. The alloys were melted *in situ* and the melt temperatures at the onset of solidification were monitored by controlling the electrical wiring. Approaching the wanted melt temperature, the controlled water flow at the bottom of the mold was initiated, thus inducing longitudinal heat flow along the vertical direction.

With a view to determining the thermal parameters during solidification, the temperature evolution at different positions along the casting length (5; 10; 15; 20; 30; 50 and 70 mm from the cooled bottom of the casting) were monitored via the output of fine type J thermocouples (0.2 mm diameter wire). All thermocouples were connected by coaxial cables to a data logger interfaced with a computer and the temperature data were collected at a frequency of 100 Hz. Each casting was sectioned along its longitudinal direction, which is parallel to the direction of solidification, mechanically

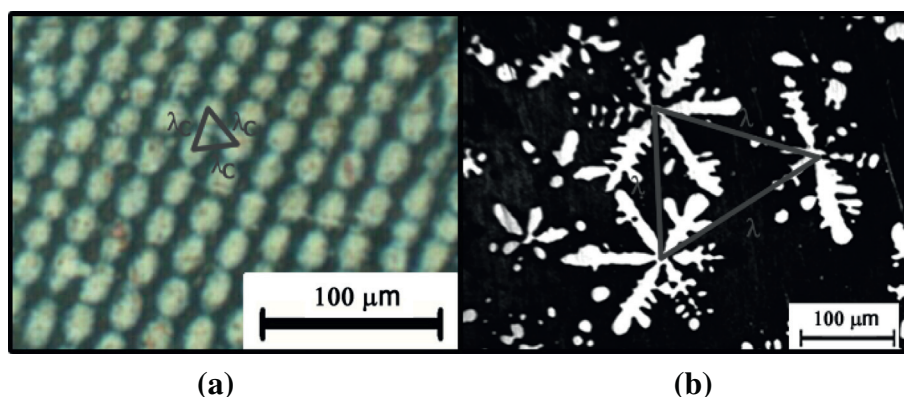


Fig. 2. Technique used for measurement of cellular (λ_c) and interphase (λ_i) spacings in the microstructure: the triangle method: (a) Zn–0.8 wt%Ag alloy and (b) Zn–8.0 wt%Ag alloy.

polished with abrasive papers and subsequently etched with an acid solution of 95 mL ethanol and 5 mL HCl to reveal the macrostructure. Selected transverse sections (perpendicular to the growth direction) of the directionally solidified castings were polished and etched with the Palmerton's reagent (40 g CrO₃; 1.5 g Na₂SO₄ and 200 mL of distilled water) to reveal the microstructure. Image processing systems Neophot 32 (Carl Zeiss, Esslingen, Germany) and Leica Quantimet 500 MC (Leica Imaging systems Ltd., Cambridge, England) were used to obtain the optical micrographs and to measure the experimental cellular (λ_c) and interphase (λ) spacings, which were measured by the triangle method [10] according to the schematic representation of Fig. 2. At least 40 measurements were performed for each selected section.

X-ray diffraction (XRD) measurements were carried out with a view to determining the phases forming the alloys microstructures. XRD patterns were obtained with a 2-theta range from 20° to 90°, Cu K α radiation with a wave-length, λ , of 0.15406 nm. In order to investigate the occurrence of macrosegregation the castings were also sectioned into transverse slices and a square central part was cut by the use of a precision saw into pieces of approximately 1.0 mm and investigated by a Rigaku Rix 3100 X-ray Fluorescence Spectrometer to estimate its average concentration

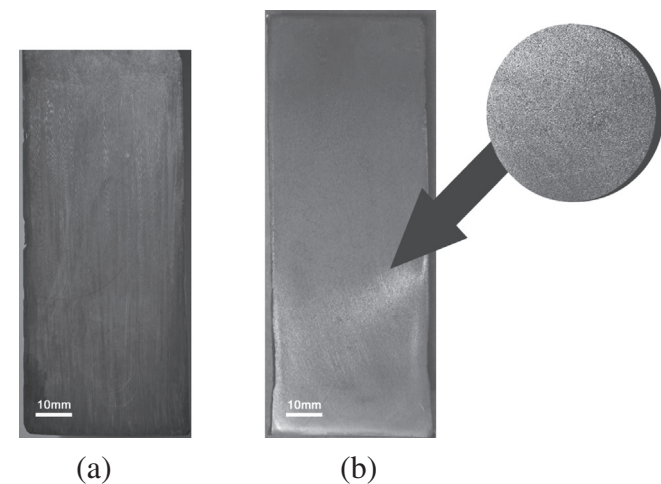


Fig. 3. (a) Columnar macrostructure of the Zn 0.8 wt%Ag alloy casting and (b) typical macrostructure of both Zn-3.2wt%Ag and Zn-8wt% Ag alloys castings, formed by fine equiaxed grains.

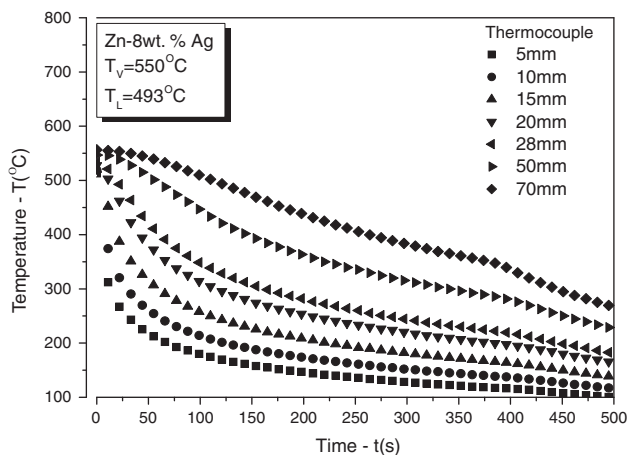


Fig. 4. Experimental cooling curves at different positions along the casting length during the unidirectional solidification of the Zn 8 wt%Ag alloy. T_v is the melt temperature at the onset of solidification and T_L is the liquidus temperature.

through an area of 100 mm² probe. Microhardness test were also performed on transverse sections of the samples using a test load of 200 g and a dwell time of 10 s. The adopted Vickers microhardness is the average of about 20 measurements on each sample.

3. Results and discussion

In Fig. 3a it can be seen that, for an alloy located in the mono-phasic range of dilute alloy compositions (Zn-0.8 wt%Ag alloy) the resulting DS macrostructure has been characterized by fine

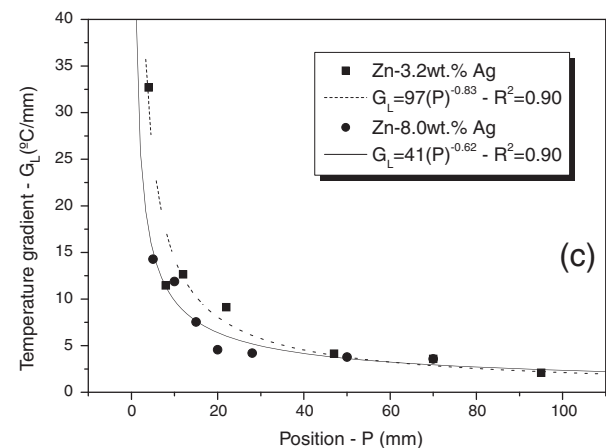
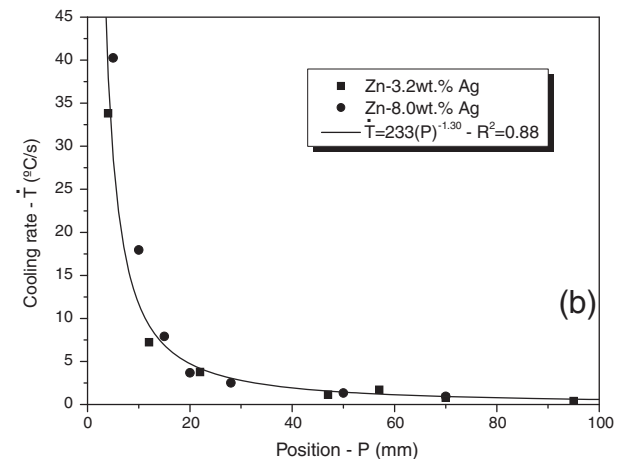
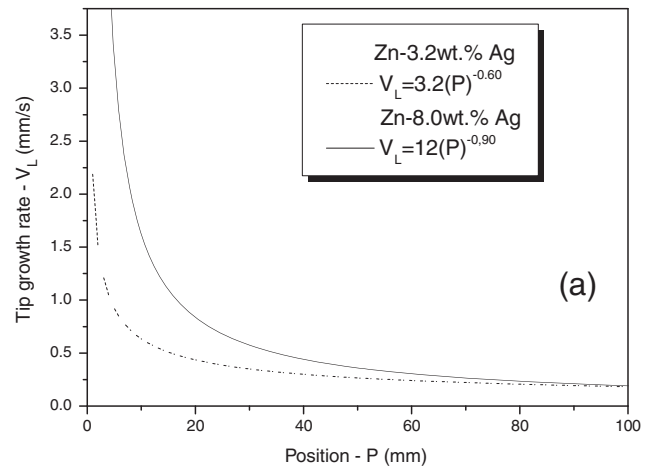


Fig. 5. Thermal parameters as a function of position from the cooled bottom of the casting during transient upward unidirectional solidification: (a) tip growth rate, (b) cooling rate and (c) temperature gradient.

columnar grains aligned with the heat flow direction. In contrast, the typical macrostructure of both the hypoperitectic (3.2 wt%Ag) and the hyperperitectic (8 wt%Ag) alloys is formed by fine equiaxed grains, which prevail in the entire casting, as shown in Fig. 3b. It seems that the increase in the alloy Ag content favors the nucleation frequency, which induces a copious nucleation ahead the solidification front promoting the growth of equiaxed grains.

A typical plot of experimental cooling curves for thermocouples placed along the castings length during the directional solidification (DS) of the alloys investigated is shown in Fig. 4 for the Zn 8 wt%Ag alloy casting. The thermal parameters (V_L , \dot{T} and G_L), have been determined by appropriate experimental thermal data. The thermocouples readings have been used to generate a plot of position from the casting cooled bottom as a function of time corresponding to the *liquidus* front passing by each thermocouple. A technique involving the empirical fit of a power function to the experimental data points was used to generate the experimental function of position vs. time. The derivative of this function with respect to time has yielded values for the tip growth rate, V_L (Fig. 5a). The cooling rate (\dot{T}) profile was calculated by considering the thermal data recorded immediately after the passage of the *liquidus* front by each thermocouple (Fig. 5b). The thermal gradient, G_L , has been obtained from the relationship between the cooling rate and tip growth rate, i.e., $\dot{T} = G_L V_L$, as shown in Fig. 5c. It can be observed in Fig. 5(a) and (b) that the use of a water-cooled mold imposes higher values of tip growth rates and cooling rates near the casting surface and a decreasing profile along the casting length due to the increasing thermal resistance of the solidified shell with distance from the cooled surface. Despite the difference in the experimental laws $V_L = f(P)$ and $G_L = f(P)$ associated with each alloy composition, it can be seen that when considering the thermal parameters that synthesizes these two parameters, i.e. the

cooling rate, a same function $\dot{T} = f(P)$ applies to both peritectic alloys examined.

The typical microstructure of the examined peritectic alloys, which solidified under non-equilibrium transient conditions, is formed by dispersed dendritic crystals of the primary ϵ phase (Zn_3Ag) in a matrix of the peritectic product phase η (solid solution of Ag in Zn) that grows below the peritectic temperature. Transverse optical micrographs are shown in Fig. 6 for both compositions examined, at different positions along the castings length and with the corresponding experimentally determined cooling rate and growth rate. Despite the wide range of solidification cooling rates associated with these microstructures (from about 1 °C/s to 20 °C/s), they are similar in morphology but differ on the size of the primary ϵ dendritic crystals and their distribution throughout the matrix, parameterized by the interphase spacing λ (also depicted in Fig. 6). It is observed that these spacings experience a significant increase with the distance from the heat-extracting surface located at the bottom of the mold. Xu et al. [16] carried out a study on microstructural evolution of both hypoperitectic and hyperperitectic Zn–Ag alloys under a wide range of growth rates and reported that the typical microstructure formed by primary dendrites of ϵ surrounded by η can be replaced with $(\eta + \epsilon)$ having a plate like morphology, with or without ϵ dendrites for growth rates higher than a critical value that increases with increase in the alloy Ag content. In the present study no evidence of plate-like morphology has been observed, even for the highest cooling rate examined (20 °C/s). However, in a previous study on the directional growth of a monophasic Zn–0.8 wt%Ag alloy by some of the present authors [18], a plate-like cellular morphology was reported to occur for $\dot{T} > 10$ °C/s. Brito et al. [13] in a recent study on transient directional solidification of Zn–Cu peritectic alloys also reported the occurrence of plate-like cellular morphology for a hypoperitectic alloy for cooling rates higher than 16 °C/s.

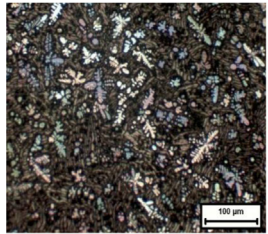
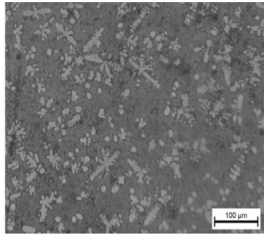
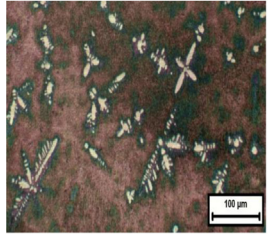
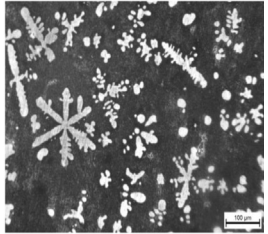
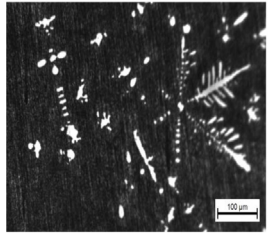
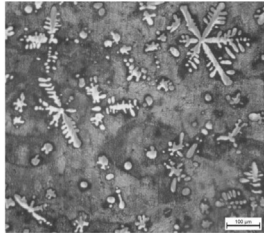
Zn-3.2wt.% Ag (Transverse section)	Data	Zn-8wt.% Ag (Transverse section)	Data
	Position: 6 mm \dot{T} : 23 °C/s V_L : 1.1 mm/s λ : 73 μ m		Position: 10 mm \dot{T} : 11.7 °C/s V_L : 1.5 mm/s λ : 71 μ m
	Position: 30 mm \dot{T} : 2.8 °C/s V_L : 0.41 mm/s λ : 102 μ m		Position: 50 mm \dot{T} : 1.4 °C/s V_L : 0.35 mm/s λ : 129 μ m
	Position: 70 mm \dot{T} : 0.9 °C/s V_L : 0.25 mm/s λ : 182 μ m		Position: 70 mm \dot{T} : 0.9 °C/s V_L : 0.26 mm/s λ : 163 μ m

Fig. 6. Transverse microstructures of the Zn–Ag peritectic alloys examined: (a) Zn–3.2 wt%Ag (hypoperitectic) and (b) Zn–8 wt%Ag (hyperperitectic), where: P is the distance from the heat-extracting surface at the bottom of the mold, \dot{T} is the cooling rate, V_L is the growth rate and λ is the interphase spacing.

In order to correlate the interphase spacing (λ) measured from the aforementioned microstructures with solidification thermal parameters, they are plotted as a function of V_L , $V_L^{-0.25} G_L^{-0.125}$ and \dot{T} in Figs. 7(a)–(c), respectively. The average, minimum and maximum values of λ are plotted in these figures; with the lines representing power function fits to the experimental scatters.

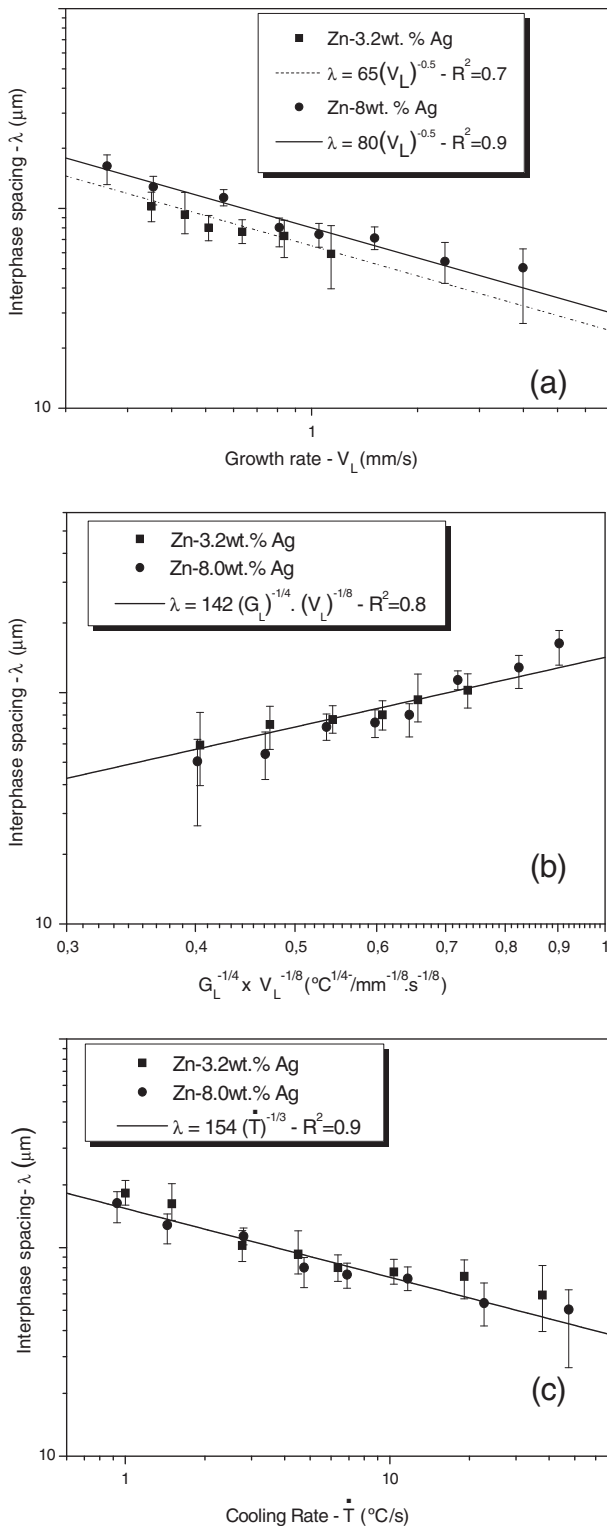


Fig. 7. Correlation between interphase spacing and: (a) tip growth rate; (b) $(G_L)^{-1/4} \times (V_L)^{-1/8}$ and (c) cooling rate, for the Zn-3.2 wt%Ag and Zn-8 wt%Ag alloys. R^2 is the coefficient of determination.

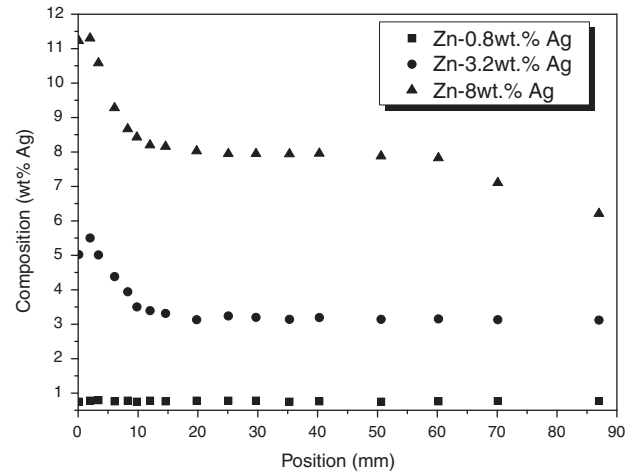


Fig. 8. Experimental macrosegregation profiles along the castings length.

As can be observed in Fig. 7(a) two experimental growth laws relate the interphase spacing to the tip growth rate (V_L) for the Zn-3.2 wt%Ag (hypoperitectic) and Zn-8.0 wt%Ag alloys (hyperperitectic). On the other hand, an important factor to be noted is that the classical lamellar eutectic growth law proposed by Jackson and Hunt [21], $\lambda^2 V = \text{constant}$, also applies to the growth of peritectic Zn–Ag alloys under transient heat flow conditions. Xu et al. [17] also reported results relating the interphase spacing of hypoperitectic and hyperperitectic Zn–Ag alloys to the growth rate during both Bridgman and laser remelting experiments. They plotted the experimental results of both experiments in single graphs, for any alloy examined, and also concluded that $\lambda V^{1/2}$ is essentially constant for a given alloy composition, and that the constant varied from 259 to 159 $\mu\text{m}^{3/2} \text{s}^{-1/2}$ for hypoperitectic and hyperperitectic alloys, respectively. It is important to observe that by mixing the results of both experiments, they are also mixing two different growth conditions; steady-state heat flow conditions (Bridgman: variable V and constant $G = 15 \text{ }^{\circ}\text{C}/\text{mm}$) and transient solidification (laser remelting). During Bridgman growth, solidification is highly controlled and the substantial controllable thermal variables, G_L and V_L , are kept constants and are they are essentially independent of each other. If a different experimental value would be adopted for G_L , a given λ value would be related to a different V_L . Furthermore, the adopted growth rate during laser remelting experiments was that of the laser beam scanning velocity. It is theoretically accepted that during laser remelting the onset of solidification at the bottom of the liquid pool occurs at a growth rate that approaches zero, and that it increases rapidly over the pool depth approaching a limiting value at the top of the laser trace that can reach the value of the laser beam rate [22]. Zhang et al. [23] in a study on laser remelting of monophasic and peritectic Zn–Ag alloys reported that both the intercellular spacing and the interphase spacing, which characterizes each alloy, respectively, decrease linearly with increase in laser scanning velocity. It seems that the adopted combination of theoretical growth rates (the laser beam rate) with results of steady-state growth under a constant thermal gradient ($G_L = 15 \text{ }^{\circ}\text{C}/\text{mm}$) cannot be considered an appropriate approach permitting reliable numerical constants of experimental growth laws for Zn–Ag peritectic alloys ($\lambda V^{1/2} = \text{constant}$) to be derived. In fact, Xu et al. remarked that the values of their experimental constants are higher than those reported in the literature for Ti–Al and Ni–Al peritectic alloys (27 and 45 $\mu\text{m}^{3/2} \text{s}^{-1/2}$, respectively) [24,25] and much higher than that of hyperperitectic Al–Cu alloys (9.4 $\mu\text{m}^{3/2} \text{s}^{-1/2}$) [26]. In the present study, the corresponding constants can be derived from the experimental laws of Fig. 7a, which for the growth law in the form $\lambda V^{1/2}$ and V in $\mu\text{m} \text{ s}^{-1}$

are given by 2.06 and 2.53 $\mu\text{m}^{3/2} \text{s}^{-1/2}$, for the hypoperitectic and hyperperitectic alloys, respectively. These values are much lower than those reported by Xu et al. [17] for Zn–Ag alloys.

It seems that more consistent experimental growth laws should encompass both the growth rate and the thermal gradient. The dependence of λ with the thermal parameters is expressed by an equation of the type $\lambda = \text{constant} (V_L^{-1/4} G_L^{-1/8})$ in Fig. 7(b). The expression has been proposed originally by Calberg and Bergman [27] for the growth of monotectic alloys and was recently validated by Silva et al. [28,29] against experimental results of directional transient solidification of hypomonotectic, monotectic and hypermonotectic Al–Bi alloys. As shown in Fig. 7b, such relationship can also be applied to the growth of peritectic Zn–Ag alloys, and represented by the same function: $\lambda = 142(G_L)^{-1/4}(V_L)^{-1/8}$ for both the hypoperitectic and hyperperitectic alloys examined in the present study.

In transient solidification, which encompasses most of the industrial solidification processes, G_L and V_L are interdependent, cannot be controlled and vary freely in time. The tip cooling rate synthesizes these two variables in absence of melt convection, since $\dot{T} = (G_L V_L)$. Fig 7(c) presents a correlation between the interphase spacing and cooling rate for the Zn–3.2 wt%Ag and Zn–8.0 wt%Ag alloys and the same power type law, given by $\lambda = 154(\dot{T}^{-1/3})$, can represent the experimental scatter of both alloys.

In order to examine the long range segregation along the directionally solidified castings lengths, the concentration profiles of Ag of both peritectic alloys examined in the present study are depicted in Fig. 8, compared with that of a Zn–Ag alloy within the monophasic range of compositions (Zn–0.8 wt%Ag alloy). It can be observed that the dilute Zn–Ag alloy does not present macrosegregation, having an essentially constant Ag concentration. On the other hand with increasing Ag content (Zn–3.2 wt%Ag and Zn–8.0 wt%Zn peritectic alloys) inverse solute segregation profiles are produced, which are quite significant from the cooled surface of the casting up to about 10 mm from this surface. The partition coefficients of both alloys examined is >1 , which causes rejection of Ag at the solidification interface. Since Ag (10,490 kg/m^3) is denser than Zn (7140 kg/m^3) [30], and solidification was carried out vertically upwards, the solute enriched liquid close to the solidification interface tends to be driven toward the casting bottom, thus inducing positive Ag segregation at regions closer to the bottom of the casting.

The effects of both length scale of the microstructures and macrosegregation on hardness, can be seen in Fig. 9a and c, where (HV) is plotted as a function of position (P) along the casting length, for the Zn–0.8 wt%Ag and both Zn–3.2 wt%Ag/Zn–8.0 wt%Ag peritectic alloys, respectively. It can be seen in Fig. 9a that an increase in P leads to a decrease in microhardness of the Zn–0.8 wt%Ag alloy (monophasic). Since no macrosegregation occurred during solidification of this alloy, the parameter affecting hardness has to be linked to microstructural features, such as the microstructure spacing. In a previous study of some of the present authors it was shown that this alloy exhibited a cellular morphology along the entire casting during transient directional solidification [18]. Fig. 9b depicts the evolution of HV with the measured cellular spacing along the casting length. It can be observed that the microhardness decreases with increase in λ_c and that the dependence of HV on $\lambda_c^{-1/2}$ can be represented by a Hall–Petch type equation given by $\text{HV} = 35 + 82(\lambda_c)^{-1/2}$. The monophasic Zn0.8 wt%Ag alloy is characterized essentially by regular cells of η phase along almost the entire DS casting, except for regions quite close to the cooled surface of the casting (for $\dot{T} > 10 \text{ }^\circ\text{C}/\text{s}$), as aforementioned, where a plate-like cellular morphology is observed [18]. The lower the cells size, the larger is the area of cell boundaries blocking dislocations. The increase in hardness may be associated mainly with the reduction in the cell size, despite the different cell morphology

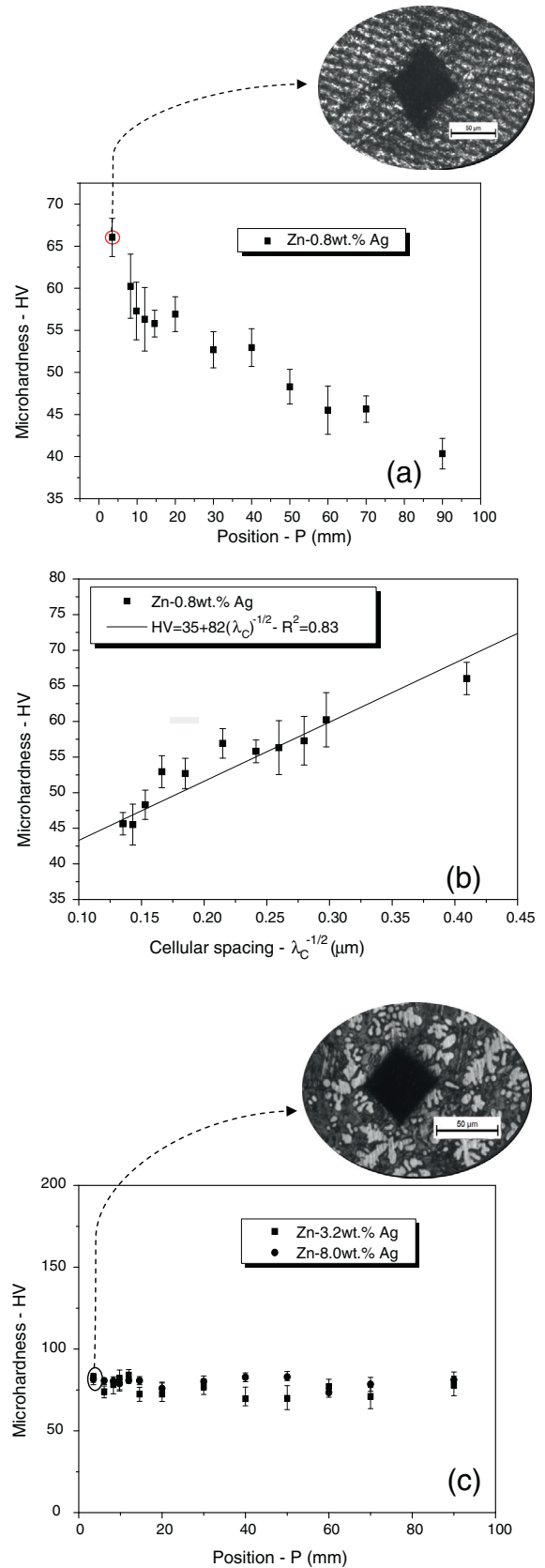


Fig. 9. Vickers microhardness (HV) as a function of position in casting (a) Zn–0.8 wt%Ag alloy; (b) HV as a function of the cellular spacing for the Zn–0.8 wt%Ag alloy and (c) HV vs. P for the 3.2–wt%Ag and Zn–8wt%Ag alloys.

(close to the casting surface) and the decrease in the intensity of the residual ϵ phase (Zn_3Ag) with the decrease in the cooling rate,

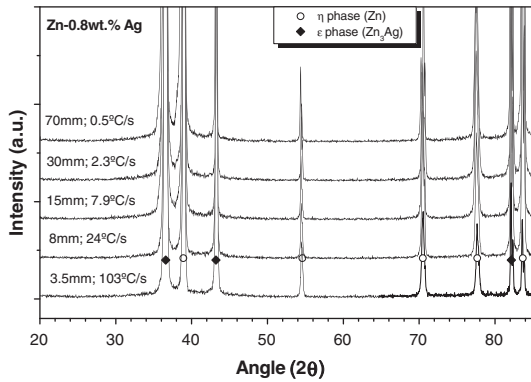
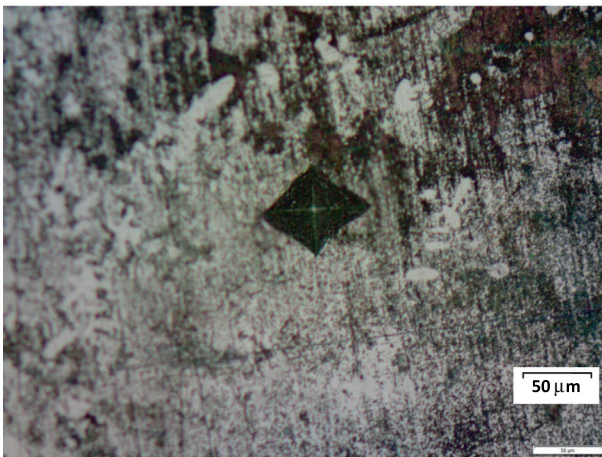


Fig. 10. Typical X-ray diffraction (XRD) patterns at different positions along the Zn–0.8wt%Ag casting length, associated with the corresponding cooling rate during solidification.



(a)



(b)

Fig. 11. Microhardness of individual phases of the Zn–3.2wt%Ag alloy (a) phase ϵ (Zn_3Ag), $HV = (75 \pm 8.0)$ and (b) phase η , $HV = (71 \pm 11.0)$.

as shown by X-ray diffractograms in Fig. 10. In previous studies on a Bi–Ag eutectic solder alloy [31] and on a ternary Al–Fe–Ni alloys [32], it was also shown that hardness can be associated with cellular and primary dendritic arm spacings by Hall–Petch type equations. In contrast, for the Zn–3.2 wt%Ag and Zn–8.0 wt%Ag

peritectic alloys, the microhardness is essentially constant along the casting length and a same average value (of about 76 HV, as shown in Fig. 9c) can be associated with the experimental scatter of both peritectic alloys. This occurs in spite of the Ag content of Zn–3.2 wt%Ag hypoperitectic alloy being less than half of that of the hyperperitectic alloy (Zn–8.0 wt%Ag) and the occurrence of positive segregation at regions close to the castings surfaces of both alloys, as shown in Fig. 8. The individual measurement of hardness in both phases forming the microstructures, shown in Fig. 11, indicates that these phases, η and ϵ (Zn_3Ag) have very similar hardness, i.e. $HV = (71 \pm 11.0)$ and $HV = (75 \pm 8.0)$, respectively. This explains the essentially constant hardness profile exhibited in Fig. 9c.

4. Conclusions

1. It was shown that during unidirectional solidification of peritectic Zn–Ag alloys, under non-equilibrium transient heat flow conditions, the peritectic reactions is stifled and the resultant microstructure is formed by dispersed dendritic crystals of the primary ϵ phase (Zn_3Ag) in a matrix of the peritectic product phase η that grows below the peritectic temperature. Experimental growth laws are proposed relating the interphase spacing of the peritectic alloys to solidification thermal parameters (growth rate, thermal gradient and cooling rate).
2. The macrostructure of both hypoperitectic and hyperperitectic alloys examined is characterized by fine equiaxed grains along the entire unidirectionally solidified castings, while for a single-phase Zn–Ag alloy casting a macrostructure of fine columnar grains prevailed. It was shown that a single-phase Zn–Ag alloy did not present macrosegregation, having an essentially constant Ag concentration along the casting length, however, with increasing Ag content (Zn–3.2 wt%Ag and Zn–8.0 wt%Ag alloys) inverse solute segregation profiles are produced, which are quite significant from the cooled surface of the casting up to about 10 mm from this surface.
3. Despite the segregation profiles and the alloying differences of the hypoperitectic and hyperperitectic alloys examined, the average microhardnesses of these alloys was shown to be similar along the castings lengths, and independent of the local interphase spacing. This was attributed to the similar hardness of both phases forming the microstructures of these alloys. In contrast, for the single phase alloy the microhardness (HV) was shown to increase with decrease in the cellular spacing (λ_c) and a Hall–Tech type experimental equation is proposed relating HV to λ_c .

Acknowledgements

The authors acknowledge the financial support provided by FAPESP – São Paulo Research Foundation, Brazil (Grants 2013/09267-0; 2012/08494-0; 2012/16328-2) and CNPq (The Brazilian Research Council).

References

- [1] Kerr HW, Kurz W. Solidification of peritectic alloys. *Int Mater Rev* 1996;41:129–64.
- [2] Yasuda H, Ohnaka I, Tokieda K, Notake N. Peritectic solidification. In: Cantor B, O'Reilly K, editors. *Solidification and Castings*. Bristol, UK: IOP Publishing Ltd.; 2003. p. 160–73.
- [3] Ha HP, Hunt JD. A numerical and experimental study of the rate of transformation in three directionally grown peritectic systems. *Metall Mater Trans* 2000;31A:29–34.
- [4] Brito C, Siqueira CA, Spinelli JE, Garcia A. Cellular growth during transient directional solidification of Zn-rich Zn–Cu monophasic and peritectic alloys. *J Phys Chem Solids* 2012;73:1173–81.

- [5] Tokieda K, Yasuda H, Ohnaka I. Formation of banded structures in Pb–Bi peritectic alloys. *Mater Sci Eng A* 1999;262:238–45.
- [6] Liu D, Li X, Su Y, Luo L, Zhang B, Guo J, et al. Directional solidification of Cu–20Sn alloy at low speed: from peritectic coupled growth to banding. *Mater Lett* 2011;65:1628–31.
- [7] Su Y, Wang M, Lin X, Huang W. Researches on lamellar structures in the unidirectional solidified Zn–2 wt%Cu peritectic alloy. *Mater Lett* 2004;58:2670–4.
- [8] Su Y, Lin X, Wang M, Xue L, Huang W. Lamellar structures in laser surface remelted Zn–Cu peritectic alloy under ultra-high temperature gradient. *Scripta Mater* 2004;51:397–403.
- [9] Hu X, Yan H, Chen W, Li S, Fu H. Effect of sample diameter on primary and secondary dendrite arm spacings during directional solidification of Pb–26 wt%Bi hypoperitectic alloy. *Rare Metals* 2011;30:424–31.
- [10] Kaya H, Böyük U, Engin S, Çadırli E, Marasli N. Measurements of microhardness and thermal and electrical properties of the binary Zn–0.7 wt%Cu hypoperitectic alloy. *J Electron Mater* 2010;39:303–11.
- [11] Ma D, Li Y, Ng SC, Jones H. Unidirectional solidification of Zn-rich Zn–Cu peritectic alloys – I. microstructure selection. *Acta Mater* 2000;48:419–31.
- [12] Ma D, Li Y, Ng SC, Jones H. Unidirectional solidification of Zn-rich Zn–Cu peritectic alloys – II. Microstructural length scales. *Acta Mater* 2000;48:1741–51.
- [13] Brito C, Siqueira CA, Spinelli JE, Garcia A. Effects of cell morphology and macrosegregation of directionally solidified Zn-rich Zn–Cu alloys on the resulting microhardness. *Mater Lett* 2012;80:106–9.
- [14] Osório WR, Brito C, Peixoto LC, Garcia A. Electrochemical behavior of Zn-rich Zn–Cu peritectic alloys affected by macrosegregation and microstructural array. *Electrochim Acta* 2012;76:218–28.
- [15] Uhlmann DR, Chadwick GA. Unidirectional solidification of melts producing the peritectic reaction. *Acta Metall* 1961;9:835–40.
- [16] Xu W, Feng YP, Li Y, Li ZY. Cellular growth of Zn-rich Zn–Ag alloys processed by rapid solidification. *Mater Sci Eng A* 2004;373:139–45.
- [17] Xu W, Feng YP, Li Y, Zhang GD, Li ZY. Rapid solidification behavior of Zn-rich Zn–Ag peritectic alloys. *Acta Mater* 2002;50:183–93.
- [18] Dias M, Brito C, Bertelli F, Garcia A. Cellular growth of single-phase Zn–Ag alloys unidirectionally solidified. *Mater Chem Phys* 2014;143:895–9.
- [19] Rocha OL, Siqueira CA, Garcia A. Cellular spacings in unsteady-state directionally solidified Sn–Pb alloys. *Mater Sci Eng A* 2003;361:111–8.
- [20] Rosa DM, Spinelli JE, Ferreira IL, Garcia A. Cellular/dendritic transition and microstructure evolution during transient directional solidification of Pb–Sb alloys. *Metall Mater Trans A* 2008;39A:2161–74.
- [21] Jackson KA, Hunt JD. Lamellar and rod eutectic growth. *Trans Metall Soc AIME* 1966;236:1129–42.
- [22] Bertelli F, Meza ES, Goulart PR, Cheung N, Riva R, Garcia A. Laser remelting of Al–1.5 wt%Fe alloy surfaces: numerical and experimental analyses. *Opt Laser Eng* 2011;49:490–7.
- [23] Zhang G, Li Z, Xu W, Li Y. Laser resolidification of Zn-rich Zn–Ag peritectic alloys. *Trans Nonferrous Met Soc China* 2002;12:433–6.
- [24] Busse P, Meissen F. Coupled growth of the peritectic α and the peritectic γ phases in binary titanium aluminides. *Scripta Mater* 1997;36:653–8.
- [25] Lee JH, Verhoeven JD. Peritectic formation in the Ni–Al system. *J Cryst Growth* 1994;144:353–66.
- [26] Gill SC, Kurz W. Rapidly solidified Al–Cu alloys I: experimental determination of the microstructure-selection map. *Acta Metall Mater* 1993;41:3563–73.
- [27] Calberg T, Bergman A. On the formation of irregular monotectic structures. *Scripta Metall* 1985;19:333–6.
- [28] Silva AP, Spinelli JE, Garcia A. Microstructural evolution during upward and downward transient directional solidification of hypomonotectic and monotectic Al–Bi alloys. *J Alloys Compd* 2009;480:485–93.
- [29] Silva AP, Spinelli JE, Manginck-Noel N, Garcia A. Microstructural development during transient directional solidification of a hypermonotectic Al–Bi alloy. *Mater Des* 2010;31:4584–91.
- [30] <http://www.webelements.com> (accessed 16 01 2014).
- [31] Spinelli JE, Silva BL, Garcia A. Microstructure, phases morphologies and hardness of a Bi–Ag eutectic alloy for high temperature soldering applications. *Mater Des* 2014;58:482–90.
- [32] Canté MV, Brito C, Spinelli JE, Garcia A. Interrelation of cell spacing, intermetallic compounds and hardness on a directionally solidified Al–1.0Fe–1.0Ni alloy. *Mater Des* 2013;51:342–6.